
Article:
Hunter, S.J. orcid.org/0000-0002-9280-1969, Chohan, P., Varlas, S. orcid.org/0000-0002-4171-7572 et al. (1 more author) (2024) Effect of temperature, oil type, and copolymer concentration on the long-term stability of oil-in-water Pickering nanoemulsions prepared using diblock copolymer nanoparticles. Langmuir, 40 (7). pp. 3702-3714. ISSN 0743-7463

https://doi.org/10.1021/acs.langmuir.3c03423

LANGMUIR

pubs.acs.org/Langmuir Article

Effect of Temperature, Oil Type, and Copolymer Concentration on the Long-Term Stability of Oil-in-Water Pickering Nanoemulsions Prepared Using Diblock Copolymer Nanoparticles

Saul J. Hunter,* Priyanka Chohan, Spyridon Varlas, and Steven P. Armes*

Cite This: *Langmuir* 2024, 40, 3702−3714 Read Online

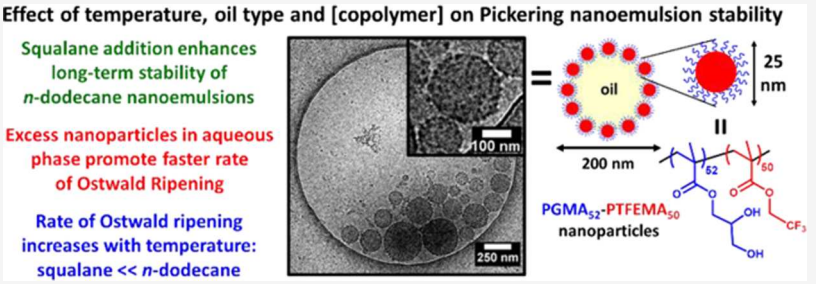

ABSTRACT: A poly(glycerol monomethacrylate) (PGMA) precursor was chain-extended with 2,2,2-trifluoroethyl methacrylate (TFEMA) via reversible addition−fragmentation chain transfer (RAFT) aqueous emulsion polymerization. Transmission electron microscopy (TEM) studies confirmed the formation of well-defined $PGMA_{52}$−$PTFEMA_{50}$ spherical nanoparticles, while dynamic light scattering (DLS) studies indicated a *z*-average diameter of 26 ± 6 nm. These sterically stabilized diblock copolymer nanoparticles were used as emulsifiers to prepare oil-in-water Pickering nanoemulsions: either *n*-dodecane or squalane was added to an aqueous dispersion of nanoparticles, followed by high-shear homogenization and high-pressure microfluidization. The Pickering nature of such nanoemulsion droplets was confirmed via cryo-transmission electron microscopy (cryo-TEM). The long-term stability of such Pickering nanoemulsions was evaluated by analytical centrifugation over a four-week period. The *n*-dodecane droplets grew in size significantly faster than squalane droplets: this is attributed to the higher aqueous solubility of the former oil, which promotes Ostwald ripening. The effect of adding various amounts of squalane to the *n*-dodecane droplet phase prior to emulsification was also explored. The addition of up to 40% (v/v) squalane led to more stable nanoemulsions, as judged by analytical centrifugation. The nanoparticle adsorption efficiency at the *n*-dodecane−water interface was assessed by gel permeation chromatography when using nanoparticle concentrations of 4.0, 7.0, or 10% w/w. Increasing the nanoparticle concentration not only produced smaller droplets but also reduced the adsorption efficiency, as confirmed by TEM studies. Furthermore, the effect of varying the nanoparticle concentration (2.5, 5.0, or 10% w/w) on the long-term stability of *n*-dodecane-in-water Pickering nanoemulsions was explored over a four-week period. Nanoemulsions prepared at higher nanoparticle concentrations were more unstable and exhibited a faster rate of Ostwald ripening. The nanoparticle adsorption efficiency was monitored for an aging nanoemulsion prepared at a copolymer concentration of 2.5% w/w. As the droplets ripened over time, the adsorption efficiency remained constant (∼97%). This suggests that nanoparticles desorbed from the shrinking smaller droplets and then readsorbed onto larger droplets over time. Finally, the effect of temperature on the stability of Pickering nanoemulsions was examined. Storing these Pickering nanoemulsions at elevated temperatures led to faster rates of Ostwald ripening, as expected.

INTRODUCTION

Pickering emulsions are oil or water droplets that are stabilized by solid particles, such as silica, clays, or latexes.[1−3] Such emulsions offer various advantages over conventional surfactant-stabilized emulsions, including greater long-term stability, more reproducible formulations, reduced foaming problems, and lower toxicity.[3] Unlike surfactant molecules, particles are normally considered to be irreversibly adsorbed at the oil−water interface, which reduces the interfacial area and hence lowers the free energy. The surface wettability of the particles dictates whether oil-in-water (O/W) or water-in-oil (W/O) Pickering emulsions are formed.[3−5]

Pickering nanoemulsions comprise either oil or water droplets of 50−500 nm diameter that are stabilized using

Received: November 8, 2023
Revised: January 7, 2024
Accepted: January 8, 2024
Published: February 5, 2024

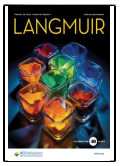

https://doi.org/10.1021/acs.langmuir.3c03423
Langmuir 2024, 40, 3702−3714

nanoparticles.[6−15] They are readily prepared via high-pressure microfluidization of Pickering macroemulsions provided that sufficient excess nanoparticles are present to stabilize the additional surface area that is generated when producing much finer droplets.[6,16] The final droplet diameter typically depends on both the applied pressure and the number of passes through a commercial microfluidizer.[16] Under optimized conditions, droplet diameters of less than 200 nm can be achieved.[6,16−19] Given their much higher surface area per unit mass, nanoemulsions offer more active formulations than conventional emulsions, which may be useful for applications in cosmetics,[20] drug delivery,[21] agrochemicals,[22,23] and food technology.[24,25]

Pickering nanoemulsions are relatively insensitive to gravitational creaming (or sedimentation) owing to their relatively small droplet size. However, their relatively high surface area makes them prone to droplet growth via Ostwald ripening.[15,26−42] For O/W nanoemulsions, This involves the diffusion of oil molecules from smaller droplets through the aqueous continuous phase to larger droplets over time. Although there are many literature reports on the formation of copolymer- or surfactant-stabilized nanoemulsions, there are surprisingly few studies focused on Pickering nanoemulsions.[6−9,12−18,43−46] This is no doubt because the Pickering emulsifier should be typically 5−10 times smaller than the mean droplet diameter.[16] Thus, droplets of (say) 200 nm diameter require nanoparticles of 20−40 nm diameter. With the exception of silica sols, such nanoparticles are not widely available as concentrated dispersions. Moreover, they must also be capable of surviving high-shear homogenization and high-pressure microfluidization.[13,18]

Polymerization-induced self-assembly (PISA) offers an efficient synthetic route to a wide range of diblock copolymer nanoparticles of tunable surface wettability.[47−54] Typically, aqueous PISA formulations involve growing a water-insoluble polymer chain from one end of a water-soluble polymer precursor.[19,48,55−62] The resulting amphiphilic diblock copolymer chains undergo *in situ* micellar nucleation to produce a concentrated colloidal dispersion of sterically stabilized nanoparticles. The most common copolymer morphology is spheres and the mean diameter can be as low as 10−20 nm diameter.[56,60,63−65] Thus aqueous PISA enables the convenient synthesis of hydrophilic spherical nanoparticles that are suitable for the preparation of Pickering nanoemulsions.[13,16−18,27,43]

For example, Thompson and co-workers examined the relative stability of a series of *n*-alkane-in-water Pickering nanoemulsions prepared using sterically stabilized nanoparticles comprising a hydrophilic poly(glycerol monomethacrylate) (PGMA) block and a hydrophobic poly(2,2,2-trifluoroethyl methacrylate) (PTFEMA) block.[16,27] Analytical centrifugation studies confirmed that nanoemulsions prepared using oils with higher aqueous solubility (e.g., *n*-octane or *n*-decane) were more susceptible toward Ostwald ripening during storage for up to 7 days at 20 °C. Conversely, nanoemulsions prepared using either *n*-dodecane or *n*-tetradecane exhibited minimal droplet growth under the same conditions.

Recently, we explored the effect of varying the nanoparticle concentration on the long-term stability of *n*-dodecane-in-water Pickering nanoemulsions, which were prepared using either 5 or 10% w/w poly(*N*,*N*′-dimethylacrylamide)-poly(diacetone acrylamide) ($PDMAC_{77}$−$PDAAM_{40}$) nanoparticles.[18] Analytical centrifugation studies indicated a gradual evolution from unimodal to bimodal droplet size distributions on storage for 8 weeks at 20 °C, with a more rapid increase in droplet size being observed for nanoemulsions prepared at higher nanoparticle concentrations. This was attributed to more efficient mass transport of oil molecules through the aqueous phase mediated by excess (non-adsorbed) nanoparticles.

Herein we explore the effect of varying the temperature, nanoparticle concentration, and oil type on the rate of Ostwald ripening of a series of oil-in-water Pickering nanoemulsions prepared using $PGMA_{52}$−$PTFEMA_{50}$ nanoparticles to stabilize either *n*-dodecane or squalane droplets.

EXPERIMENTAL SECTION

Materials. All reagents were used as received, unless otherwise stated. Glycerol monomethacrylate (GMA; 99.8% purity) was obtained from GEO Specialty Chemicals (Hythe, U.K.). 2,2,2-Trifluoroethyl methacrylate (TFEMA), 4,4′-azobis(4-cyanopentanoic acid) (ACVA), *n*-dodecane, squalane, and ethanol were all purchased from Sigma-Aldrich (U.K.). Each monomer was passed through a basic alumina column to remove its inhibitor prior to use. 2-Cyano-2-propyl dithiobenzoate (CPDB) was purchased from Strem Chemicals Ltd. (Cambridge, U.K.). d_6-Acetone and d_4-methanol (CD_3OD) were purchased from Goss Scientific Instruments Ltd. (Cheshire, U.K.). *N*,*N*-Dimethylformamide (DMF) was purchased from Fisher Scientific (U.K.). Deionized water (pH 6) was used for all studies involving aqueous solutions.

Methods. *Synthesis of a $PGMA_{52}$ Precursor via RAFT Solution Polymerization in Ethanol.* GMA (30.1 g, 0.186 mol), CPDB (0.589 g, 2.66 mmol; target DP = 70), ACVA (0.149 g, 0.532 mmol; CPDB/ACVA molar ratio = 5.0), and anhydrous ethanol (45.9 g) were weighed into a 100 mL round-bottom flask. The resulting solution was deoxygenated by purging with a stream of nitrogen gas for 30 min at 20 °C before the flask was immersed in an oil bath at 70 °C for 165 min with continuous stirring. The polymerization was quenched by removal of the flask from the oil bath and exposure of the reaction mixture to air while cooling the flask to 20 °C. A GMA conversion of 72% was determined by ^{1}H NMR spectroscopy by comparing the integrated monomer vinyl signals at 5.7 and 6.2 ppm with the five pendent PGMA proton signals at 3.7−4.3 ppm. The crude polymer was purified by precipitation into a ten-fold excess of DCM (three times) and then freeze-dried from water. A mean DP of 52 was determined via end-group analysis using ^{1}H NMR spectroscopy (d_4-methanol) by comparing the integrated peaks of the aromatic protons assigned to the dithiobenzoate chain ends at 7.4−7.9 ppm to the five pendent GMA protons at 3.7−4.3 ppm. DMF GPC analysis (using a UV detector set at 298 nm) indicated an M_n of 13 100 g mol^{-1} and an M_w/M_n of 1.21.

Synthesis of $PGMA_{52}$−$PTFEMA_{50}$ Diblock Copolymer Nanoparticles via RAFT Aqueous Emulsion Polymerization of TFEMA. A $PGMA_{52}$ precursor (2.50 g, 0.304 mmol), ACVA (0.0167 g, 0.0608 mmol; $PGMA_{52}$/ACVA molar ratio = 5.0), and deionized water (45.6 g) were added to a 100 mL round-bottom flask, and then degassed with a stream of nitrogen gas for 30 min at 20 °C. TFEMA (2.16 mL, 0.0152 mol; target DP = 50 at 10% w/w solids) was degassed separately using an ice bath to minimize evaporation and then injected into the round-bottom flask prior to its immersion in an oil bath at 70 °C for 6 h. The TFEMA polymerization was quenched by exposing the reaction mixture to air while cooling the flask to ambient temperature. ^{19}F NMR spectroscopy analysis in d_6-acetone indicated more than 99% TFEMA conversion. DMF GPC analysis (using a UV detector set at 298 nm) indicated an M_n of 22 000 g mol^{-1} and an M_w/M_n of 1.19.

Preparation of $PGMA_{52}$−$PTFEMA_{50}$-Stabilized Pickering Macroemulsions using High-Shear Homogenization. An aqueous dispersion of $PGMA_{52}$−$PTFEMA_{50}$ nanoparticles (2.40 mL, 7.0% w/w) was added to a 14 mL glass vial and homogenized with *n*-

https://doi.org/10.1021/acs.langmuir.3c03423
Langmuir 2024, 40, 3702−3714

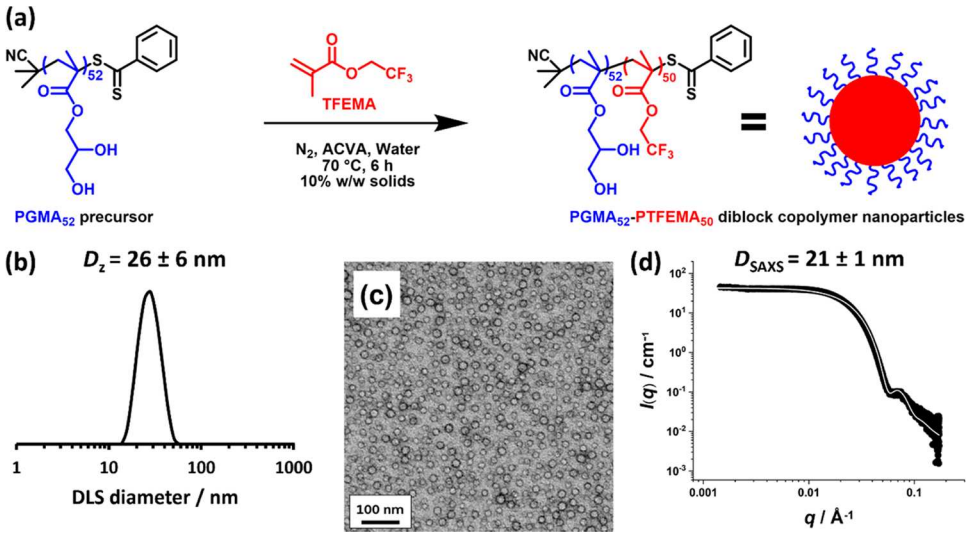

Figure 1. (a) Synthesis of $PGMA_{52}$–$PTFEMA_{50}$ diblock copolymer spheres via the RAFT aqueous emulsion polymerization of TFEMA at 70 °C. (b) DLS intensity-average particle size distribution obtained for a 0.1% w/w aqueous dispersion of $PGMA_{52}$–$PTFEMA_{50}$ diblock copolymer nanoparticles. (c) TEM image recorded after drying a 0.2% w/w aqueous dispersion of $PGMA_{52}$–$PTFEMA_{50}$ nanoparticles at 20 °C. (d) SAXS pattern recorded for a 1.0% w/w aqueous dispersion of $PGMA_{52}$–$PTFEMA_{50}$ nanoparticles at 20 °C. The data fit (solid white line) was obtained using a spherical micelle model.[67,68]

dodecane (0.60 mL) at 13 500 rpm for 2 min at 20 °C using an IKA Ultra-Turrax T-18 homogenizer equipped with a 10 mm dispersing tool. The same protocol was used to prepare squalane-in-water Pickering macroemulsions. A series of Pickering macroemulsions were also prepared by systematically varying the nanoparticle concentration from 2.5 to 10% w/w.

Preparation of $PGMA_{52}$–$PTFEMA_{50}$-Stabilized Pickering Nanoemulsions using High-Pressure Microfluidization. A Pickering macroemulsion (3.0 mL) was further processed with the aid of an LV1 microfluidizer (Microfluidics). The applied pressure was 20 000 psi, and each macroemulsion was passed through the LV1 ten times to afford well-defined Pickering nanoemulsions.

NMR Spectroscopy. All ^{1}H and ^{19}F NMR spectra were recorded in either d_4-methanol or d_6-acetone using a Bruker Avance-400 spectrometer operating at 400 MHz.

Gel Permeation Chromatography (GPC). An Agilent 1260 Infinity GPC system equipped with a differential refractive index detector and a UV detector was used to determine the number-average molecular weight (M_n), weight-average molecular weight (M_w), and dispersity (M_w/M_n) for each (co)polymer. Two Agilent PL-gel 5 μm mixed-C columns and a guard column were connected in series to this GPC system. Unless otherwise stated, high-performance liquid chromatography (HPLC) grade DMF containing 10 mM LiBr was used as the eluent. GPC analysis was performed at 60 °C using a constant flow rate of 1.0 mL min^{-1}. A series of near-monodisperse poly(methyl methacrylate) calibration standards with M_p values ranging from 800 g mol^{-1} to 2 200 000 g mol^{-1} were used to calculate molecular weights and dispersities. All (co)polymer samples were diluted to 1.0% w/w using the GPC eluent and chromatograms were analyzed using Agilent GPC/SEC software.

Dynamic Light Scattering (DLS). Intensity-average size distributions and z-average hydrodynamic diameters, D_z, were obtained at a scattering angle of 173° using a Malvern Zetasizer Nano ZS instrument. Dilute (0.1% w/w) dispersions of $PGMA_{52}$–$PTFEMA_{50}$ nanoparticles and various Pickering nanoemulsions were analyzed by using disposable plastic cuvettes at 20 °C. In each case, the results were averaged over three consecutive runs.

Transmission Electron Microscopy (TEM). Copper/palladium TEM grids (Agar Scientific, U.K.) were surface-coated with a thin film of amorphous carbon. If required, grids were subjected to a plasma glow discharge for 30 s to produce a hydrophilic surface. One droplet of an aqueous dispersion of nanoparticles (0.2% w/w, 10 μL) or a nanoemulsion (0.5% v/v, 10 μL) was placed on a grid for 1 min, after which any remaining solution was removed by blotting with filter paper. Subsequently, an aqueous droplet of uranyl formate (0.75% w/w, 10 μL) was placed on the sample-loaded grid for 20 s, and the excess stain was removed by blotting. Each grid was carefully dried using a vacuum hose. Images were recorded using an FEI Tecnai Spirit microscope operating at 80 kV and equipped with a Gatan 1kMS600CW CCD camera.

Cryogenic Transmission Electron Microscopy (cryo-TEM). Imaging was performed using an FEI Tecnai Arctica microscope operating at an acceleration voltage of 200 kV. Cryo-TEM samples were prepared by depositing 5 μL of a 0.5% w/w dodecane-in-water or squalane-in-water Pickering nanoemulsion onto a plasma-treated Quantifoil holey carbon-coated copper grid, followed by blotting for approximately 4 s and then plunging into a pool of liquid ethane to vitrify the sample using a Leica EM GP automatic plunge freezer (25 °C, 99% humidity). Transfer of the vitrified grids into a precooled cryo-TEM holder was performed at −196 °C prior to microscopic analysis.

Analytical Centrifugation (LUMiSizer). Droplet size distributions were analyzed using a LUMiSizer analytical photocentrifuge (LUM GmbH, Berlin, Germany) at 20–60 °C. Measurements were conducted on 1.0% v/v Pickering nanoemulsions using 2 mm path length polyamide cells at 500, 1000, 2000, and 4000 rpm for 200 profiles each (with 10 s between each profile). The LUMiSizer instrument uses space- and time-resolved extinction profiles (STEP) technology to measure the intensity of transmitted near-infrared light as a function of time and position over the entire cell length. The gradual progression of transmission profiles contained information on the rate of creaming, which allowed assessment of the droplet size distribution. The droplet density is an essential input parameter for analytical centrifugation measurements. For the nanoemulsion aging studies, this parameter was taken to be either 0.75 g cm^{-3} (for *n*-dodecane droplets) or 0.81 g cm^{-3} (for squalane droplets). Such densities ignore the contribution from the relatively dense $PGMA_{52}$–$PTFEMA_{50}$ nanoparticles adsorbed at the surface of each oil droplet. However, this approximation is acceptable for the present study, given that only relative changes in the droplet size distribution are assessed over time.

Small-Angle X-ray Scattering (SAXS). SAXS experiments were conducted on 1.0% w/w aqueous dispersions of $PGMA_{52}$–$PTFEMA_{50}$ nanoparticles and the corresponding 1.0% v/v squalane-in-water Pickering nanoemulsion at the ESRF (station ID02, Grenoble, France) using monochromatic X-ray radiation (λ =

https://doi.org/10.1021/acs.langmuir.3c03423
Langmuir 2024, 40, 3702–3714

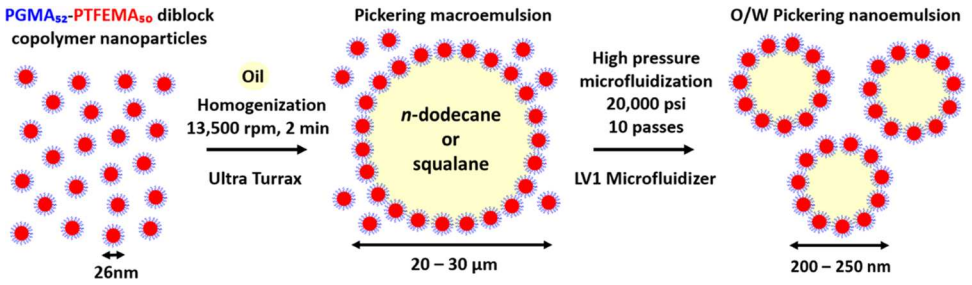

Figure 2. Schematic representation for the formation of O/W Pickering nanoemulsions using $PGMA_{52}$−$PTFEMA_{50}$ nanoparticles as a Pickering emulsifier. First, high-shear homogenization of 2.5−10% w/w aqueous dispersions of such nanoparticles with 20% v/v *n*-dodecane (or squalane) resulted in the formation of a Pickering macroemulsion with a mean droplet diameter of 20−30 μm. Then this precursor macroemulsion was passed ten times through a high-pressure microfluidizer at 20 000 psi to produce the desired O/W Pickering nanoemulsion with a mean droplet diameter of approximately 200−250 nm.

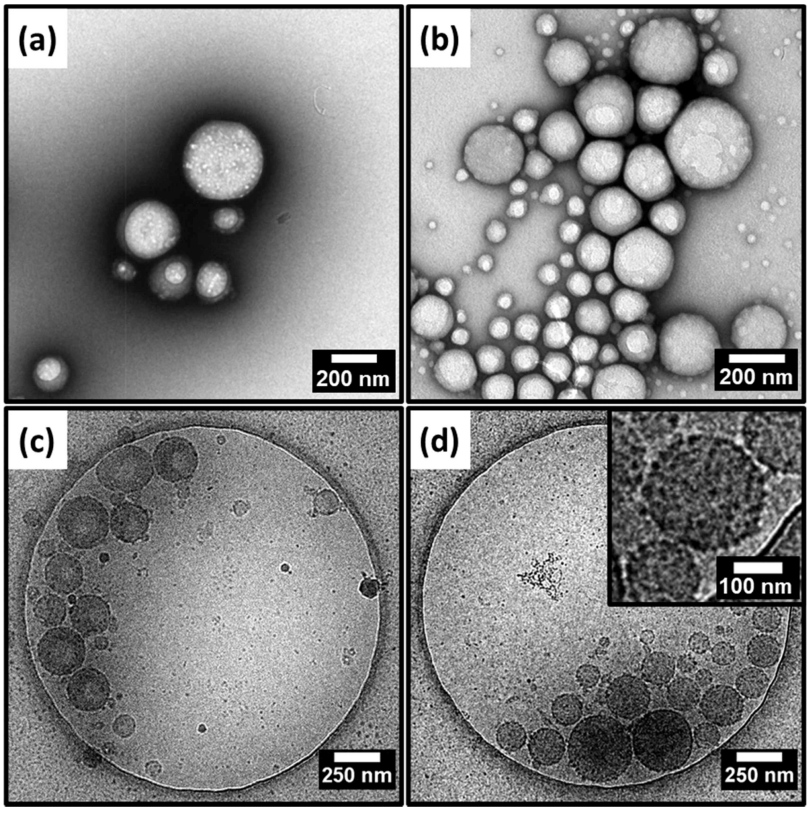

Figure 3. Representative (a, b) conventional TEM and (c, d) cryo-TEM images obtained for freshly prepared (a, c) *n*-dodecane-in-water or (b, d) squalane-in-water Pickering nanoemulsions prepared via high-pressure microfluidization using 7.0% w/w $PGMA_{52}$−$PTFEMA_{50}$ nanoparticles and 20% v/v oil. Nanoemulsion preparation conditions: applied pressure = 20 000 psi for 10 passes using an LV1 microfluidizer.

0.0995 nm; q range = 0.002−0.15 Å^{-1}, where q is the length of the scattering vector and θ is one-half of the scattering angle, such that $q = 4\pi \sin\theta/\lambda$) and an Eiger24M two-dimensional detector (Dectris, Switzerland). A flow-through glass capillary (2 mm diameter) was connected to a syringe and a waste container via plastic tubing and mounted horizontally on the beamline stage; this setup was used as a sample holder. Scattering data were reduced using standard routines provided by the beamline and were further analyzed using Irena SAS macros for Igor Pro.[66]

RESULTS AND DISCUSSION

Synthesis and Characterization of $PGMA_{52}$−$PTFEMA_{50}$ Diblock Copolymer Nanoparticles. A PGMA precursor with a target DP of 70 was prepared via RAFT solution polymerization in ethanol using a CPDB RAFT agent and an ACVA initiator. To ensure retention of the end-group fidelity, this polymerization was quenched after 165 min, which produced a GMA conversion of 72%. After purification of the crude polymer, its mean DP was determined to be 52 by end-group analysis using ^{1}H NMR spectroscopy (see Figure S1). DMF GPC studies of this precursor indicated an M_n of 13 100 g mol^{-1} and an M_w/M_n of 1.21, as shown in Figure S3.

$PGMA_{52}$−$PTFEMA_{50}$ diblock copolymer nanoparticles were prepared by chain-extending the water-soluble $PGMA_{52}$ precursor via RAFT aqueous emulsion polymerization of TFEMA using a protocol reported by Akpinar and co-workers.[45] The synthesis of such nanoparticles is outlined in Figure 1a. ^{19}F NMR spectroscopy analysis of the resulting diblock copolymer indicated more than 99% TFEMA conversion (the integrated residual TFEMA monomer signal at −74.34 ppm was compared to the signal assigned to the

https://doi.org/10.1021/acs.langmuir.3c03423
Langmuir 2024, 40, 3702−3714

PTFEMA block at −73.95 ppm; see Figure S2). DMF GPC studies of this diblock copolymer indicated an M_n of 22 000 g mol^{-1} and a relatively narrow molecular weight distribution (M_w/M_n = 1.19); see Figure S3. The unimodal GPC trace indicates efficient chain extension and hence minimal contamination from the unreacted $PGMA_{52}$ precursor.

DLS characterization of the nanoparticles indicated a z-average hydrodynamic diameter of 26 ± 6 nm and a relatively low DLS polydispersity of 0.05 (Figure 1b). TEM analysis confirmed a well-defined spherical morphology (Figure 1c). Since this technique is conducted under ultrahigh vacuum, only the PTFEMA cores can be observed. Digital image analysis indicated an approximate number-average diameter of 18 ± 2 nm for a population of 100 nanoparticles. Small-angle X-ray scattering (SAXS) studies reported an overall volume-average diameter of 21 ± 1 nm (Figure 1d).

Effect of Oil Solubility on the Stability of Pickering Nanoemulsions. Pickering macroemulsions were prepared by homogenizing 2.5−10% w/w aqueous dispersions of $PGMA_{52}$−$PTFEMA_{50}$ nanoparticles with 20% v/v *n*-dodecane (or squalane) for 2 min at 13 500 rpm. This produced relatively coarse oil droplets with a mean volume-average diameter of 20−30 μm. These macroemulsions were then passed ten times through a high-pressure microfluidizer at 20 000 psi, resulting in the formation of Pickering nanoemulsions of approximately 200 nm diameter. This processing step is illustrated in Figure 2. The oil volume was fixed at 20% because higher volumes might cause either phase inversion[76] or produce unstable emulsion droplets.[77] Thompson et al. reported that an applied pressure of 20 000 psi was optimal for the preparation of stable o/w Pickering nanoemulsions when using similar $PGMA_{48}$−$PTFEMA_{50}$ nanoparticles.[70] Lower pressures produced larger, more polydisperse droplets, whereas higher pressures caused *in situ* nanoparticle disassembly, which led to droplets becoming stabilized by individual amphiphilic copolymer chains (rather than intact nanoparticles). Thompson et al. also found that at least eight passes through the microfluidizer were required to achieve a unimodal size distribution, with ten passes producing the smallest droplets. Hence, this previously optimized protocol was used to produce all of the O/W Pickering nanoemulsions reported in the present study.

In 2010, Persson et al. used commercially available silica nanoparticles to prepare a series of O/W Pickering nanoemulsions with various oils.[6] However, *n*-alkanes (including *n*-dodecane) invariably led to highly unstable droplets; only squalene (a naturally occurring, highly water-insoluble oil) produced relatively stable droplets. Thompson and co-workers subsequently investigated the long-term stability of a series of O/W Pickering nanoemulsions prepared using $PGMA_{48}$−$PTFEMA_{50}$ nanoparticles to stabilize *n*-octane, *n*-decane, *n*-dodecane, or *n*-tetradecane droplets.[71] Increasing the *n*-alkyl chain length of the oil significantly lowered its solubility in the aqueous phase and, as a result, reduced the rate of Ostwald ripening.[71]

Accordingly, two Pickering nanoemulsions were prepared by using a 7.0% w/w aqueous dispersion of $PGMA_{52}$−$PTFEMA_{50}$ nanoparticles and 20% v/v *n*-dodecane (or squalane) for TEM studies. Representative TEM images obtained for freshly prepared nanoemulsions are shown in Figure 3a,b. Both the oil droplet phase and the aqueous continuous phase evaporate completely under ultrahigh vacuum conditions, leaving only the nanoparticles that were adsorbed at the surface of the oil droplets. These spherical nanoparticle superstructures are comparable in size to the mean DLS diameter of the original oil droplets. Furthermore, close inspection reveals the presence of the individual nanoparticles, which confirms the genuine Pickering nature of such nanoemulsions. Finally, there are relatively few nanoparticles remaining in the background, indicating a relatively high adsorption efficiency.

Cryo-TEM images obtained for the same two Pickering nanoemulsions are shown in Figure 3c,d. For this imaging technique, both the oil droplets and the aqueous continuous phase are subjected to rapid freezing rather than evaporation. Again, the frozen droplets have mean diameters that are comparable to those reported by DLS and there is also some evidence for the presence of adsorbed nanoparticles at the droplet surface.

To calculate the adsorption efficiency of the nanoparticles on the oil droplets, a calibration plot of integrated UV GPC signal intensity (recorded at λ = 298 nm) against nanoparticle concentration was constructed (see Figure S4).[43] This involved analyzing the UV chromatograms recorded after serial dilution of an aqueous dispersion of $PGMA_{52}$−$PTFEMA_{50}$ nanoparticles using DMF. This is a good solvent for both PGMA and PTFEMA and hence results in nanoparticle dissolution to form soluble diblock copolymer chains. This linear calibration plot was used to determine the concentration of non-adsorbed nanoparticles remaining in the aqueous supernatant after centrifugation of the nanoemulsion at 13 000 rpm for 15 min. This causes creaming (rather than sedimentation) of the oil droplets. Subtracting the concentration of non-adsorbed nanoparticles from the initial nanoparticle concentration enables calculation of the adsorption efficiency, A_{eff}, which was determined to be 97% for a freshly prepared *n*-dodecane-in-water nanoemulsion. Next, the mean packing efficiency, *P*, for the adsorbed layer of nanoparticles surrounding each oil droplet was calculated using a core−shell model reported by Balmer et al.[69] Assuming a contact angle of 0° for nanoparticle adsorption at the oil−water interface, *P* was determined to be 50% for a Pickering nanoemulsion prepared using *n*-dodecane at a $PGMA_{52}$−$PTFEMA_{50}$ concentration of 7% w/w. A 1.0% v/v squalane-in-water nanoemulsion was also characterized using SAXS. The resulting SAXS pattern (see Figure 4) was analyzed using the same two-population model (see the Supporting Information for further details) previously used to characterize *n*-dodecane-in-water and water-in-*n*-dodecane Pickering nanoemulsions.[13,43]

One population is represented by core−shell spheres, where the cores comprise oil droplets and the shell is formed by the adsorbed layer of nanoparticles. The second population corresponds to the particulate nature of the shell and is described by spherical micelles with a hard-sphere structure factor to account for interparticle interactions at the oil−water interface. This two-population model produced a satisfactory fit to the scattering pattern (see Figure 4) and an overall mean droplet radius of 92 ± 22 nm, which is consistent with the corresponding DLS data (D_z = 196 ± 63 nm). The mean apparent shell thickness for the adsorbed layer of nanoparticles was calculated to be approximately 8 nm, which is significantly lower than the volume-average diameter of an individual nanoparticle (~21 ± 1 nm; Figure 1d). However, this is consistent with the relatively low surface coverage of the oil droplets by the nanoparticles, which exhibit a packing efficiency of around 40%.

https://doi.org/10.1021/acs.langmuir.3c03423
Langmuir 2024, 40, 3702−3714

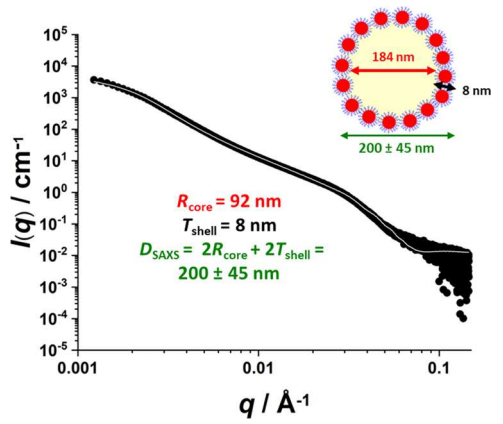

Figure 4. SAXS pattern (black circles) and corresponding data fit (solid white line) obtained for a 1.0% v/v Pickering nanoemulsion prepared using 7.0% w/w $PGMA_{52}$–$PTFEMA_{50}$ nanoparticles with squalane as the oil phase. The two-population core–shell structural model[43] used for SAXS analysis of this Pickering nanoemulsion comprises squalane droplet cores coated with an adsorbed layer of $PGMA_{52}$–$PTFEMA_{50}$ spherical nanoparticles. Nanoemulsion preparation conditions: applied pressure = 20 000 psi for 10 passes using an LV1 microfluidizer.

The droplet size distribution of each nanoemulsion was monitored over the course of four weeks via analytical centrifugation (LUMiSizer instrument). Analytical centrifugation was preferred to DLS for the study of droplet growth because it is a high-resolution technique, with oil droplets being fractionated according to their size prior to detection.[71] The data obtained from such analytical centrifugation studies are depicted in Figure 5. For such experiments, the standard deviation of the droplet size distribution is perhaps a more sensitive indicator of the relative droplet stability than the mean diameter.

Inspecting Figure 5, it is evident that the *n*-dodecane droplet size distribution becomes significantly broader after aging for 4 weeks at 20 °C. In contrast, only minimal change is observed for the analogous squalane droplets over the same time scale. This can be explained by Lifshitz–Slyozov–Wagner (LSW) theory for Ostwald ripening.[34,37,70,71] This assumes that (i) the oil phase comprises solely spherical droplets, (ii) the distance between neighboring droplets is substantially larger than the mean droplet diameter, and (iii) droplet growth is solely governed by the diffusion of oil (or water) molecules through the aqueous (or oil) phase.[79] The rate of Ostwald ripening, ω, can be calculated using eq 1, where $C(\infty)$ is the solubility of the oil phase within the aqueous phase, γ is the interfacial tension, V_m is the molar volume of the oil, D is the diffusion coefficient for the oil droplets within the aqueous phase, and ρ is the density of the oil phase.

$$\omega = \frac{dr^3}{dt} = \frac{8}{9}\left[\frac{C(\infty)\gamma V_m D}{\rho RT}\right] \quad (1)$$

According to eq 1, the rate of Ostwald ripening is proportional to the solubility of the droplet phase within the continuous phase. Thus, using a highly water-insoluble oil such as squalane (aqueous solubility = 0.012 μg dm^{-3} at 25 °C[6]) should suppress the rate of Ostwald ripening much more significantly than when using *n*-dodecane (aqueous solubility = 3.4 μg dm^{-3} at 20 °C[27]).

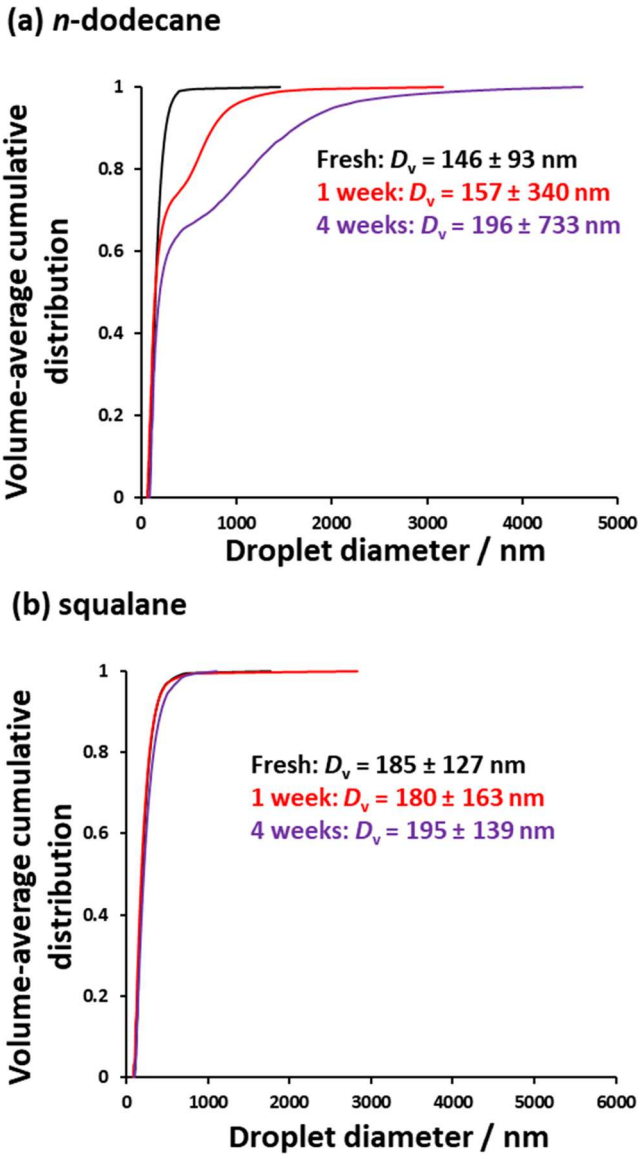

Figure 5. Volume-average cumulative distributions determined by analytical centrifugation after aging for up to 4 weeks at 20 °C: (a) an *n*-dodecane-in-water nanoemulsion and (b) a squalane-in-water nanoemulsion at 20% v/v. The harmonic mean ± standard deviation is reported for each time period. Nanoemulsion preparation conditions: applied pressure = 20 000 psi for 10 passes using an LV1 microfluidizer.

In principle, Ostwald ripening can be suppressed by adding a suitable species to the droplet phase that is highly insoluble in the continuous phase.[40,72] For example, it is well-documented that the addition of a relatively long hydrocarbon (or wax) to oil droplets enhances the stability of O/W nanoemulsions toward Ostwald ripening.[29,34,40,73] Similarly, the addition of salt to the aqueous phase is known to inhibit interdroplet mass transfer in the case of W/O emulsions.[13,74] In the present study, varying proportions of squalane (5 to 40% by volume) were added to *n*-dodecane prior to high-shear homogenization. Using analytical centrifugation to monitor the evolution of droplet size distributions over time, we can examine how the presence of squalane affects the rate of Ostwald ripening of *n*-dodecane-in-water nanoemulsions (see Figure 6). Clearly, the addition of increasing amounts of squalane progressively

https://doi.org/10.1021/acs.langmuir.3c03423
Langmuir 2024, 40, 3702–3714

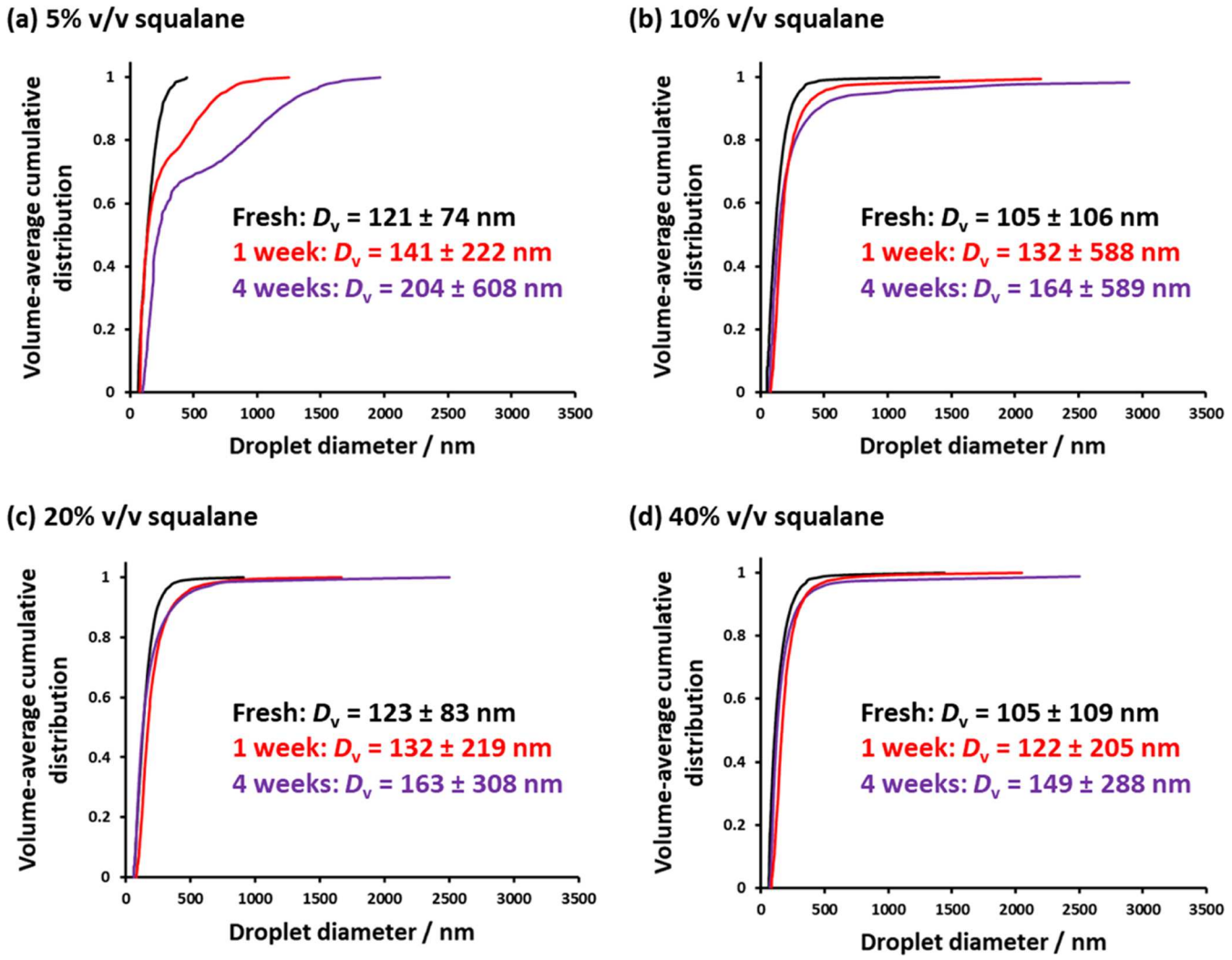

Figure 6. Volume-average cumulative distributions determined by analytical centrifugation after aging for up to 4 weeks at 20 °C: an *n*-dodecane-in-water nanoemulsion at 20% v/v containing (a) 5%, (b) 10%, (c) 20%, and (d) 40% squalane by volume. The harmonic mean ± standard deviation is reported for each time period. Nanoemulsion preparation conditions: applied pressure = 20 000 psi for 10 passes using an LV1 microfluidizer.

retards the rate of Ostwald ripening. However, this enhanced stability never matches that achieved for Pickering nanoemulsions comprising squalane alone (see Figure 5).

Effect of Copolymer Concentration on the Long-Term Stability of Pickering Nanoemulsions. Recently, Hunter and Armes reported that preparing Pickering nanoemulsions using higher copolymer concentrations led to a faster rate of Ostwald ripening, which was attributed to the excess nanoparticles facilitating oil transport through the aqueous phase.[18]

To extend this prior study, we decided to examine the effect of copolymer concentration on the adsorption efficiency, A_{eff}, the number of nanoparticles per droplet, N, and the packing efficiency, P, was determined. Furthermore, the change in nanoparticle adsorption efficiency over time was examined by using a previously reported UV GPC protocol to monitor the nanoparticle concentration remaining in the aqueous continuous phase.[18]

First, the effect of varying the nanoparticle concentration on the adsorption efficiency was examined for freshly prepared and aged nanoemulsions. Accordingly, three *n*-dodecane-in-water Pickering nanoemulsions were prepared using 2.5, 5.0, or 10% w/w $PGMA_{52}$–$PTFEMA_{50}$ nanoparticles. TEM images were recorded after drying each of the three freshly prepared nanoemulsions to observe the original nanoparticle superstructure and assess the presence of any excess non-adsorbed nanoparticles (see Figure 7). Clearly, increasing the nanoparticle concentration leads to finer droplets but at the expense of a higher proportion of non-adsorbed nanoparticles. However, such TEM studies might be prone to drying artifacts arising during sample grid preparation. Thus nanoparticle adsorption efficiencies were determined for the freshly prepared nanoemulsions using UV GPC.[43] Such experiments revealed that increasing the nanoparticle concentration reduced the adsorption efficiency; see Table 1. At lower nanoparticle concentrations, there are fewer nanoparticles available to stabilize the relatively large oil droplets, leading to an adsorption efficiency of almost 100%. At higher nanoparticle concentrations, smaller droplets are formed and the total surface area of the oil phase is higher. However, at some point the nanoparticles are present in excess. Thus some of the nanoparticles are no longer able to adsorb at the oil–water interface, which inevitably leads to lower adsorption efficiencies. As expected, there are fewer nanoparticles

https://doi.org/10.1021/acs.langmuir.3c03423
Langmuir 2024, 40, 3702−3714

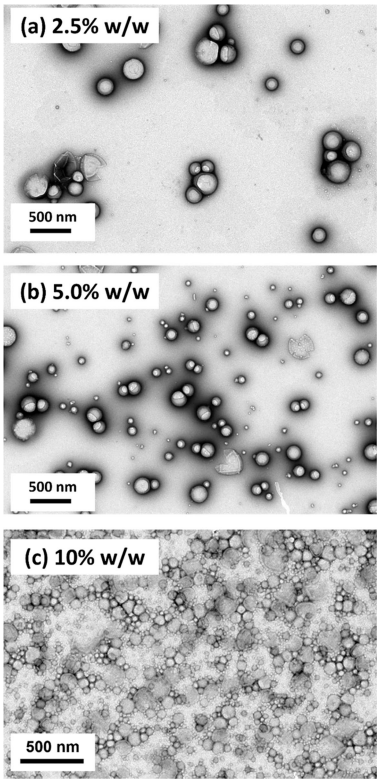

Figure 7. Representative TEM images recorded after drying freshly prepared n-dodecane-in-water Pickering nanoemulsions prepared using (a) 2.5% w/w, (b) 5.0% w/w, or (c) 10% w/w $PGMA_{52}$–$PTFEMA_{50}$ nanoparticles. Nanoemulsion preparation conditions: applied pressure = 20 000 psi for 10 passes using an LV1 microfluidizer.

Table 1. Summary of the Characterization Data Obtained for the Three *n*-Dodecane-in-Water Pickering Nanoemulsions Prepared Using 2.5, 5.0, or 10% w/w $PGMA_{52}$–$PTFEMA_{50}$ Nanoparticles[a]

nanoparticle concentration (% w/w)	D_z (nm)	D_v (nm)	A_{eff} (%)	N	P (%)
2.5	326 ± 92	350 ± 165	97	548	36
5.0	213 ± 67	199 ± 118	95	250	45
10	174 ± 60	147 ± 73	65	175	46

[a]Nanoemulsion preparation conditions: applied pressure = 20 000 psi for 10 passes using an LV1 microfluidizer. [N.B. D_z is the z-average hydrodynamic diameter as determined by DLS; D_v is the volume-average droplet diameter, as determined by analytical centrifugation; A_{eff} is the nanoparticle adsorption efficiency, as determined *by* UV GPC;[43] N is the number of nanoparticles per droplet; and P is the packing efficiency, calculated using a model reported by Balmer et al.[69]]

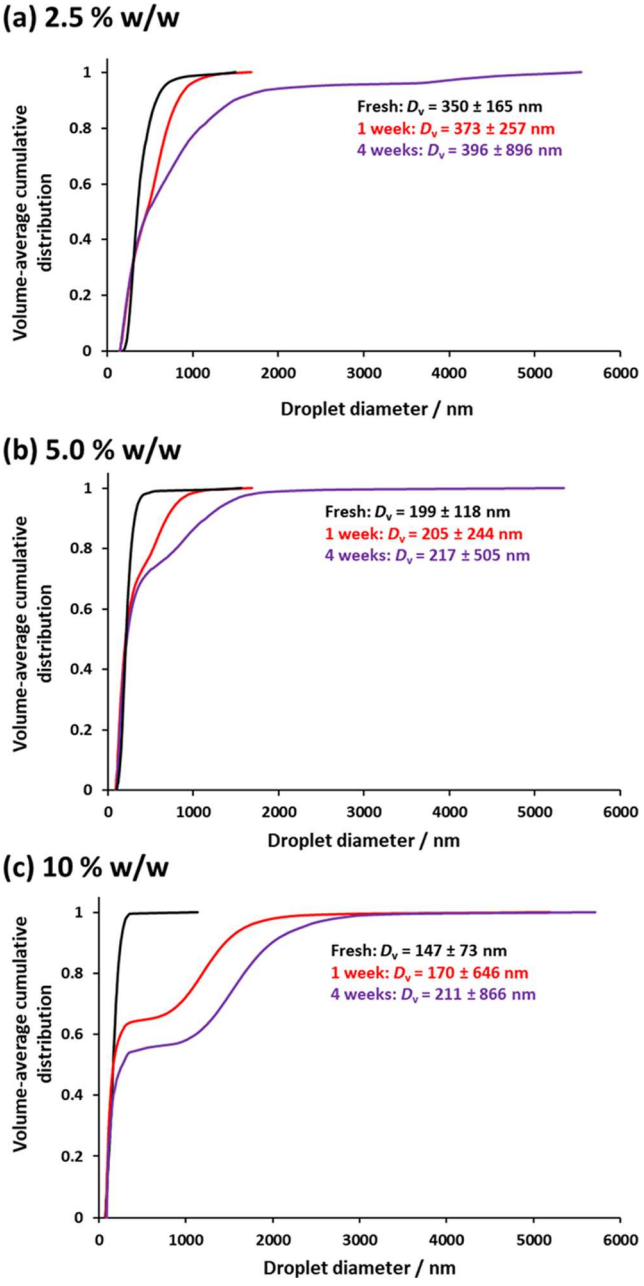

Figure 8. Volume-average cumulative distributions determined by analytical centrifugation for fresh and aged n-dodecane-in-water Pickering nanoemulsions at 20% v/v, prepared using (a) 2.5% w/w, (b) 5.0% w/w, or (c) 10% w/w $PGMA_{52}$–$PTFEMA_{50}$ diblock copolymer nanoparticles. The harmonic mean ± standard deviation is reported in each case. Nanoemulsion preparation conditions: applied pressure = 20 000 psi for 10 passes using an LV1 microfluidizer.

adsorbed per droplet, N, as the mean droplet diameter is reduced.

To determine the effect of copolymer concentration on the long-term stability of these Pickering nanoemulsions, their droplet size distributions were monitored by DLS (see Figure S5) and analytical centrifugation (see Figure 8). Perhaps surprisingly, DLS seems to be relatively insensitive to droplet growth over longer time scales compared to analytical centrifugation. Similar observations were reported by Thompson and co-workers[70,71] but the precise reason for this unexpected discrepancy is still unknown. Although the mean DLS droplet diameter did not increase significantly, the DLS polydispersity (which is a crude measure of the width of the droplet size distribution) increased approximately two-fold after aging each nanoemulsion for four weeks at 20 °C. This is consistent with broadening of the original droplet size distribution.

The analytical centrifugation data confirmed that finer droplets are indeed obtained when using higher nanoparticle concentrations. Moreover, the mean droplet diameter increases on aging each of the three nanoemulsions. This is consistent with Ostwald ripening, which is widely considered to be the

https://doi.org/10.1021/acs.langmuir.3c03423
Langmuir 2024, 40, 3702−3714

dominant mechanism for the destabilization of Pickering nanoemulsions.[71,78] Moreover, the most significant change in the droplet size distribution was observed for the nanoemulsion prepared using 10% w/w nanoparticles. One likely reason for this is the relatively small droplet radius. According to the Kelvin equation, this leads to higher oil solubility within the aqueous phase[75]

$$C(r) = C(\infty)\exp\left(\frac{2\gamma V_m}{rRT}\right) \quad (2)$$

where $C(r)$ is the solubility of the spherical droplets dispersed within the continuous phase, $C(\infty)$ is the bulk phase solubility (i.e., the solubility of an infinitely large droplet), and V_m is the molar volume of the dispersed phase. This inevitably leads to a faster rate of Ostwald ripening, as indicated by eq 1. The faster rate of Ostwald ripening for nanoemulsions prepared at higher nanoparticle concentrations can also be explained by the presence of excess nanoparticles. Such non-adsorbed nanoparticles accelerate the ripening process by enhancing the rate of mass transport of oil molecules within the aqueous phase. Furthermore, a transition from an initial unimodal size distribution to bimodal droplet size distributions is observed for nanoemulsions prepared using 5.0 and 10% w/w nanoparticles, which agrees with data previously reported by Hunter and Armes.[18] This suggests that using higher nanoparticle concentrations (more specifically, the presence of excess nanoparticles that typically arise when using higher nanoparticle concentrations) has a detrimental effect on the long-term stability of Pickering nanoemulsions.

The effect of varying the nanoparticle concentration on the adsorption efficiency was also studied over a four-week period. The same three *n*-dodecane-in-water nanoemulsions prepared using 2.5, 5.0, or 10% w/w $PGMA_{52}$–$PTFEMA_{50}$ nanoparticles were used for these experiments. Each nanoemulsion was centrifuged at 13 000 rpm for 15 min to allow creaming of the low-density oil droplets. The underlying aqueous supernatant was then analyzed via UV GPC at a fixed wavelength of 298 nm, and the calibration plot previously constructed for the $PGMA_{52}$–$PTFEMA_{50}$ nanoparticles (Figure S4) was used to determine the concentration of non-adsorbed nanoparticles. The results obtained from these experiments are summarized in Table 2.

Almost no change in adsorption efficiency was observed for the *n*-dodecane-in-water nanoemulsion prepared at a nanoparticle concentration of 2.5% w/w. At first sight, this does not appear to be consistent with the significant increase in droplet diameter that is observed over time for this nanoemulsion. Larger droplets should lead to a reduction in the overall surface area, resulting in a reduction in nanoparticle surface coverage and hence a lower adsorption efficiency. However, Ostwald ripening also results in preferential dissolution of the smaller oil droplets according to the Kelvin equation. As these finer droplets shrink over time, nanoparticle desorption from the oil–water interface should occur owing to the reduction in interfacial area. Subsequently, these nanoparticles adsorb onto the growing larger droplets to maintain their original high surface coverage. This explains the constant adsorption efficiency (~97%) that is observed over time. Since the volume-average droplet diameter increases over time and the adsorption efficiency remains essentially unchanged, the number of nanoparticles per droplet, *N*, necessarily increases. According to Table 2, there is also a modest increase in the packing efficiency, *P*. In principle, the lower interfacial curvature of the growing oil droplets enables more efficient nanoparticle packing at the oil/water interface.

Table 2. Summary of the Characterization Data Obtained after Aging the Three *n*-Dodecane-in-Water Pickering Nanoemulsions Prepared Using 2.5% w/w $PGMA_{52}$–$PTFEMA_{50}$ Nanoparticles for up to 4 weeks at 20 °C[a]

time (week)	D_v (nm)	A_{eff} (%)	N	P (%)
fresh	350	97	581	43
1	373	97	718	46
2	375	96	724	46
3	379	95	742	46
4	396	97	876	50

[a]Nanoemulsion preparation conditions: applied pressure = 20 000 psi for 10 passes using an LV1 microfluidizer. [N.B. D_v is the volume-average droplet diameter determined by analytical centrifugation; A_{eff} is the nanoparticle adsorption efficiency determined using UV GPC;[43] *N* is the number of nanoparticles per droplet; and *P* is the packing efficiency, calculated using a model reported by Balmer et al.[69]]

Effect of Temperature on the Stability of Pickering Nanoemulsions. Several studies have examined the effect of storage temperature on the stability of surfactant-stabilized nanoemulsions.[73,76−79] For example, Delmas et al.[73] reported that the rate of Ostwald ripening, ω, of O/W nanoemulsions stabilized using a non-ionic surfactant followed Arrhenius behavior according to eq 3:

$$\omega \propto \exp\left(-\frac{E}{k_B T}\right) \quad (3)$$

As far as we are aware, there have been no reports of the effect of aging Pickering nanoemulsions at elevated temperature. In view of this gap in the literature, we decided to study the effect of temperature on the rate of Ostwald ripening of *n*-dodecane-in-water Pickering nanoemulsions. The *z*-average diameter of a freshly prepared *n*-dodecane-in-water nanoemulsion diluted to 1% v/v was monitored at 10 min intervals while aging at either 20 or 60 °C using DLS. This technique was preferred to analytical centrifugation for such experiments because it enabled many measurements to be recorded over a relatively short time scale. The cube of the mean droplet radius (r^3) increased approximately linearly over time for the first 160 min (see Figure 9).

This is consistent with LSW theory for Ostwald ripening, see eq 1.[37,70,71] From the gradients of these two linear plots, the rate of Ostwald ripening ω is calculated to be 24 ± 2 $nm^3\ s^{-1}$ at 20 °C and 56 ± 3 $nm^3\ s^{-1}$ at 60 °C. Moreover, Kabalnov et al. reported that experimental ω values are systematically higher by a factor of ~2.5 compared to those calculated using LSW theory.[80] This discrepancy was attributed to the Brownian motion of emulsion droplets because LSW theory is derived for droplets trapped within a solid matrix. Thus the above experimental ω value observed at 20 °C is comparable to the theoretical value (12 $nm^3\ s^{-1}$) calculated for *n*-dodecane droplets at the same temperature.[37] Furthermore, the more than two-fold increase in ω observed at 60 °C is comparable to data reported by Delmas and co-workers for surfactant-stabilized O/W nanoemulsions aged at various temperatures ranging from 25 to 60 °C.[73] This observation was attributed to the temperature-sensitive nature of both the solubility and diffusivity of the dispersed phase.

https://doi.org/10.1021/acs.langmuir.3c03423
Langmuir 2024, 40, 3702−3714

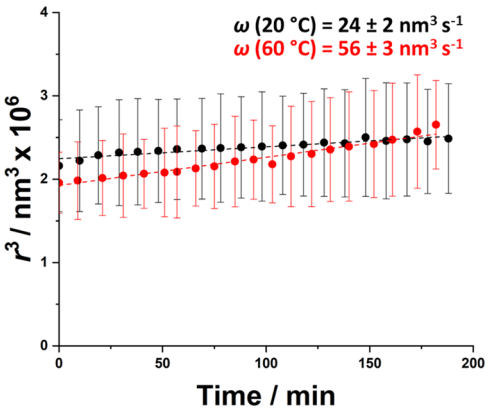

Figure 9. Variation in the cube of the mean droplet radius (r^3) over time as determined by DLS studies of aging *n*-dodecane-in-water Pickering nanoemulsions at either 20 °C (black data points) or 60 °C (red data points). Nanoemulsion preparation conditions: 7.0% w/w $PGMA_{52}$–$PTFEMA_{50}$ nanoparticles; applied pressure = 20 000 psi; 10 passes through an LV1 microfluidizer.

To further explore the effect of temperature on Ostwald ripening, we studied the *long-term* stability of the O/W Pickering nanoemulsions prepared using either *n*-dodecane or squalane. Accordingly, freshly prepared nanoemulsions were stored at either 40 or 60 °C and the droplet size distribution of each nanoemulsion was monitored over a four-week period using analytical centrifugation. Figure 10 shows the temperature-dependent stability of the Pickering nanoemulsions. Clearly, aging at 40 °C leads to the evolution of broader *n*-dodecane droplet size distributions over time. Moreover, this instability is much more discernible at 60 °C, as confirmed by optical microscopy studies (see inset images recorded for the final aged nanoemulsions). In contrast, there is essentially no change in the droplet size distributions recorded for squalane-in-water nanoemulsions aged for four weeks at 40 °C, although some increase in droplet size is detected at 60 °C.

Schatzberg[81] reported that the aqueous solubility of *n*-dodecane at 40 °C is almost twice that at 25 °C and that this temperature dependence is consistent with theoretical aqueous solubilities calculated using the Hildebrand equation.[82] Moreover, Stevenson and co-workers determined the aqueous solubility of squalane at elevated temperature (above 600 K) and pressure (greater than 150 bar).[83] Linear extrapolation of these data suggests that the aqueous solubility of squalane at

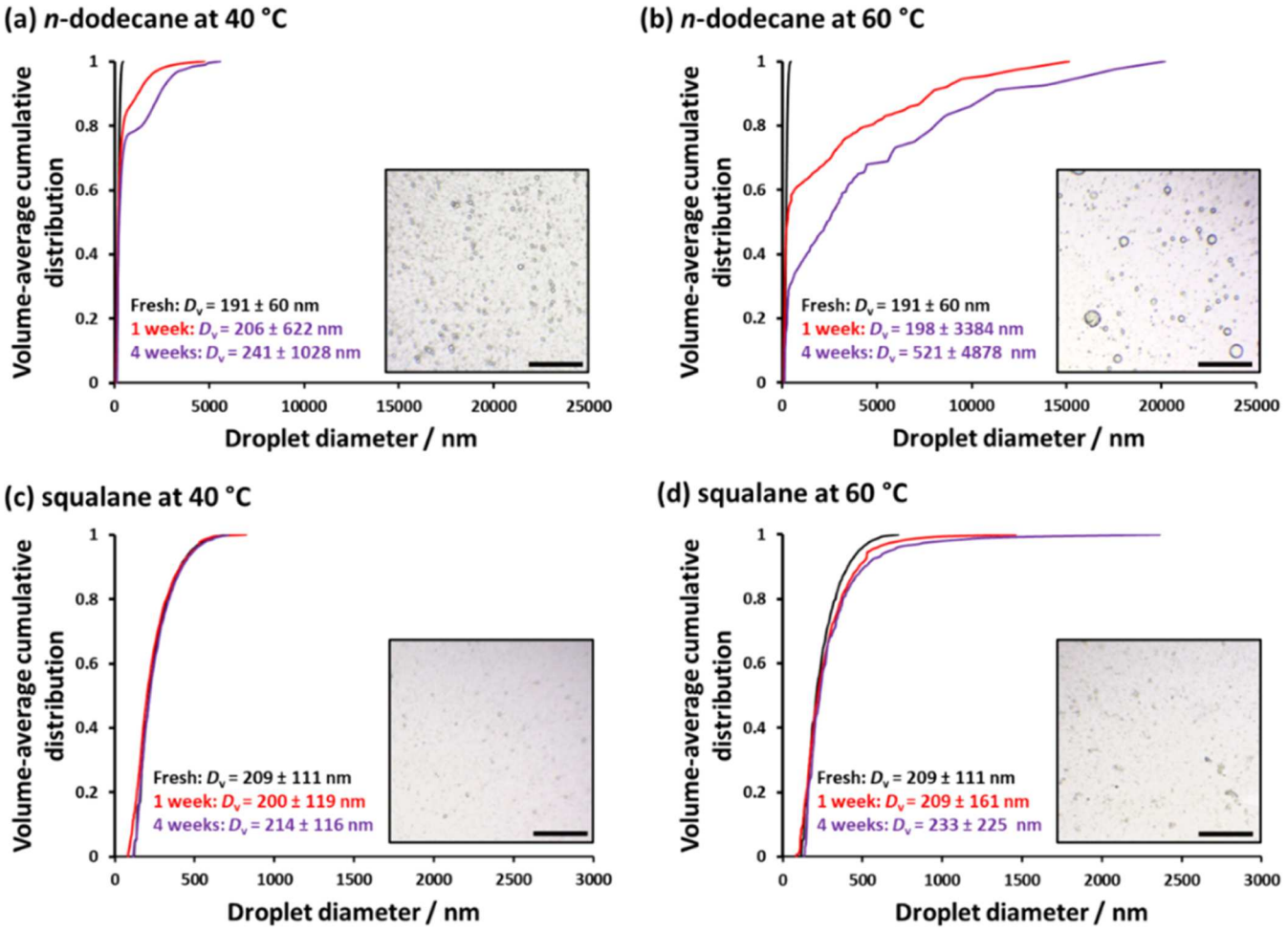

Figure 10. Volume-average cumulative droplet size distributions determined by analytical centrifugation for fresh and aged Pickering nanoemulsions prepared at 20% v/v using either (a, b) *n*-dodecane or (c, d) squalane as the droplet phase after storage at either 40 or 60 °C. The harmonic mean ± standard deviation is reported for the fresh and aged nanoemulsions. Insets show optical microscopy images recorded for each aged nanoemulsion after 4 weeks (scale bars represent 100 μm). Nanoemulsion preparation conditions: applied pressure = 20 000 psi for 10 passes using an LV1 microfluidizer.

https://doi.org/10.1021/acs.langmuir.3c03423
Langmuir 2024, 40, 3702−3714

ambient pressure is approximately 0.011 μg dm^{-3} at 20 °C, 0.014 μg dm^{-3} at 40 °C, and 0.016 μg dm^{-3} at 60 °C.

Hence the observed differing nanoemulsion stabilities simply reflect the higher aqueous solubility of *n*-dodecane compared to squalane at any given temperature plus the known temperature-dependent aqueous solubility of each oil. These experimental observations are consistent with an Ostwald ripening mechanism for droplet growth.

CONCLUSIONS

Well-defined $PGMA_{52}$–$PTFEMA_{50}$ spherical nanoparticles were synthesized via aqueous PISA for the preparation of O/W Pickering nanoemulsions by (i) high-shear homogenization and (ii) high-pressure microfluidization. The long-term stability of the resulting *n*-dodecane-in-water and squalane-in-water Pickering nanoemulsions was studied over a four-week period at 20–60 °C using analytical centrifugation. The mean droplet size increased much more rapidly when using *n*-dodecane compared to squalane. This is attributed to the higher aqueous solubility of the former oil, which leads to a faster rate of Ostwald ripening. The addition of 20 to 40% (v/v) squalane to *n*-dodecane droplets prior to emulsification leads to more stable Pickering nanoemulsions. A series of *n*-dodecane-in-water Pickering nanoemulsions were prepared using 4.0, 7.0, or 10% w/w $PGMA_{52}$–$PTFEMA_{50}$ nanoparticles to investigate the effect of nanoparticle concentration on adsorption efficiency. UV GPC was used to determine the fraction of non-adsorbed nanoparticles for each nanoemulsion. Increasing the nanoparticle concentration reduced the mean droplet size and hence lowered the adsorption efficiency from almost 100% (when using 4.0% w/w nanoparticles) to 77% (when using 10% w/w nanoparticles). The number of nanoparticles adsorbed onto each droplet was also reduced at higher nanoparticle concentrations, owing to the formation of smaller droplets. DLS and analytical centrifugation studies both show that the rate of Ostwald ripening for *n*-dodecane-in-water Pickering nanoemulsions is temperature-dependent, which is consistent with LSW theory. More specifically, the rate of Ostwald ripening at 60 °C is more than twice that at 20 °C. In contrast, squalane-in-water nanoemulsions are significantly more resistant to Ostwald ripening when aged at the same temperature over a period of four weeks. This simply reflects the differing temperature-dependent aqueous solubilities of these two model oils.

ASSOCIATED CONTENT

Supporting Information

The Supporting Information is available free of charge at https://pubs.acs.org/doi/10.1021/acs.langmuir.3c03423.

^{1}H NMR spectra for the $PGMA_{52}$ precursor and ^{1}H NMR and ^{19}F NMR spectra for the $PGMA_{52}$–$PTFEMA_{50}$ diblock copolymer; DMF GPC curves for the $PGMA_{52}$ precursor and $PGMA_{52}$–$PTFEMA_{50}$ diblock copolymer; UV GPC calibration plot for the $PGMA_{52}$–$PTFEMA_{50}$ diblock copolymer; DLS data recorded for aging *n*-dodecane-in-water Pickering nanoemulsions prepared using various concentrations of $PGMA_{52}$–$PTFEMA_{50}$ nanoparticles; details of the core–shell and spherical micelle model scattering models used for the SAXS analysis (PDF)

AUTHOR INFORMATION

Corresponding Authors

Saul J. Hunter – *School of Chemistry, Joseph Banks Laboratories, University of Lincoln, Lincoln LN6 7TS, U.K.*; orcid.org/0000-0002-9280-1969; Email: sahunter@lincoln.ac.uk

Steven P. Armes – *Department of Chemistry, University of Sheffield, Sheffield S3 7HF South Yorkshire, U.K.*; orcid.org/0000-0002-8289-6351; Email: s.p.armes@sheffield.ac.uk

Authors

Priyanka Chohan – *Department of Chemistry, University of Sheffield, Sheffield S3 7HF South Yorkshire, U.K.*

Spyridon Varlas – *Department of Chemistry, University of Sheffield, Sheffield S3 7HF South Yorkshire, U.K.*; orcid.org/0000-0002-4171-7572

Complete contact information is available at: https://pubs.acs.org/10.1021/acs.langmuir.3c03423

Author Contributions

This manuscript was written through contributions of all authors. All authors have given approval to the final version of the manuscript.

Notes

The authors declare no competing financial interest.

ACKNOWLEDGMENTS

S.P.A. acknowledges the EPSRC for an Established Career Particle Technology Fellowship (EP/R003009). The authors thank Christopher Hill and Dr. Svetomir Tzokov at the University of Sheffield Biomedical Science Electron Microscopy suite. The authors acknowledge the ESRF (beamline ID02, Grenoble, France) for synchrotron beamtime (Proposal Number SC-5315).

REFERENCES

(1) Ramsden, W. Separation of Solids in the Surface-Layers of Solutions and 'Suspensions' (Observations on Surface-Membranes, Bubbles, Emulsions, and Mechanical Coagulation). *Proc. R. Soc. Lond.* **1904**, *72*, 156–164.

(2) Pickering, S. U. CXCVI.—Emulsions. *J. Chem. Soc., Trans.* **1907**, *91*, 2001–2021.

(3) Binks, B. P. Particles as surfactants—similarities and differences. *Curr. Opin. Colloid Interface Sci.* **2002**, *7*, 21–41.

(4) Arditty, S.; Whitby, C. P.; Binks, B. P.; Schmitt, V.; Leal-Calderon, F. Some general features of limited coalescence in solid-stabilized emulsions. *Eur. Phys. J. E* **2003**, *11*, 273–281.

(5) Aveyard, R.; Binks, B. P.; Clint, J. H. Emulsions stabilised solely by colloidal particles. *Adv. Colloid Interface Sci.* **2003**, *100–102*, 503–546.

(6) Persson, K. H.; Blute, I. A.; Mira, I. C.; Gustafsson, J. Creation of well-defined particle stabilized oil-in-water nanoemulsions. *Colloids Surf., A* **2014**, *459*, 48–57.

(7) Saelices, C. J.; Capron, I. Design of Pickering Micro- and Nanoemulsions Based on the Structural Characteristics of Nanocelluloses. *Biomacromolecules* **2018**, *19*, 460–469.

(8) Kang, D. J.; Barnia, H.; Anand, S. Synthesizing Pickering Nanoemulsions by Vapor Condensation. *ACS Appl. Mater. Interfaces* **2018**, *10*, 21746–21754.

(9) Du, Z.; Li, Q.; Li, J.; Su, E.; Liu, X.; Wan, Z.; Yang, X. Self-Assembled Egg Yolk Peptide Micellar Nanoparticles as a Versatile Emulsifier for Food-Grade Oil-in-Water Pickering Nanoemulsions. *J. Agric. Food Chem.* **2019**, *67*, 11728–11740.

(10) Zhao, Q.; Jiang, L. X.; Lian, Z.; Khoshdel, E.; Schumm, S.; Huang, J. B.; Zhang, Q. Q. High internal phase water-in-oil emulsions stabilized by food-grade starch. *J. Colloid Interface Sci.* **2019**, *534*, 542−548.
(11) Xiao, Z.; Liu, Y.; Niu, Y.; Kou, X. Cyclodextrin supermolecules as excellent stabilizers for Pickering nanoemulsions. *Colloids Surf., A* **2020**, *588*, No. 124367.
(12) Yang, Z.; Wang, W.; Wang, G.; Tai, X. Optimization of low-energy Pickering nanoemulsion stabilized with montmorillonite and nonionic surfactants. *Colloids Surf., A* **2020**, *585*, No. 124098.
(13) Hunter, S. J.; Cornel, E. J.; Mykhaylyk, O. O.; Armes, S. P. Effect of Salt on the Formation and Stability of Water-in-Oil Pickering Nanoemulsions Stabilized by Diblock Copolymer Nanoparticles. *Langmuir* **2020**, *36*, 15523−15535.
(14) Gauthier, G.; Capron, I. Pickering nanoemulsions: An overview of manufacturing processes, formulations, and applications. *JCIS Open* **2021**, *4*, No. 100036.
(15) Ding, B.; Ahmadi, S. H.; Babak, P.; Bryant, S. L.; Kantzas, A. On the Stability of Pickering and Classical Nanoemulsions: Theory and Experiments. *Langmuir* **2023**, *39*, 6975−6991.
(16) Thompson, K. L.; Cinotti, N.; Jones, E. R.; Mable, C. J.; Fowler, P. W.; Armes, S. P. Bespoke Diblock Copolymer Nanoparticles Enable the Production of Relatively Stable Oil-in-Water Pickering Nanoemulsions. *Langmuir* **2017**, *33*, 12616−12623.
(17) Hunter, S. J.; Armes, S. P. Sterically Stabilized Diblock Copolymer Nanoparticles Enable Efficient Preparation of Non-Aqueous Pickering Nanoemulsions. *Langmuir* **2023**, *39*, 7361−7370.
(18) Hunter, S. J.; Armes, S. P. Long-Term Stability of Pickering Nanoemulsions Prepared Using Diblock Copolymer Nanoparticles: Effect of Nanoparticle Core Crosslinking, Oil Type, and the Role Played by Excess Copolymers. *Langmuir* **2022**, *38*, 8021−8029.
(19) Hunter, S. J.; Lovett, J. R.; Mykhaylyk, O. O.; Jones, E. R.; Armes, S. P. Synthesis of diblock copolymer spheres, worms and vesicles via RAFT aqueous emulsion polymerization of hydroxybutyl methacrylate. *Polym. Chem.* **2021**, *12*, 3629−3639.
(20) Sonneville-Aubrun, O.; Simonnet, J. T.; L'Alloret, F. Nanoemulsions: a new vehicle for skincare products. *Adv. Colloid Interface Sci.* **2004**, *108−109*, 145−149.
(21) Singh, Y.; Meher, J. G.; Raval, K.; Khan, F. A.; Chaurasia, M.; Jain, N. K.; Chourasia, M. K. Nanoemulsion: Concepts, development and applications in drug delivery. *J. Controlled Release* **2017**, *252*, 28−49.
(22) Du, Z.; Wang, C.; Tai, X.; Wang, G.; Liu, X. Optimization and Characterization of Biocompatible Oil-in-Water Nanoemulsion for Pesticide Delivery. *ACS Sustainable Chem. Eng.* **2016**, *4*, 983−991.
(23) Mustafa, I. F.; Hussein, M. Z. Synthesis and Technology of Nanoemulsion-Based Pesticide Formulation. *Nanomaterials* **2020**, *10*, No. 1608.
(24) Aswathanarayan, J. B.; Vittal, R. R. Nanoemulsions and Their Potential Applications in Food Industry. *Front. Sustainable Food Syst.* **2019**, *3*, No. 95.
(25) McClements, D. J.; Rao, J. Food-Grade Nanoemulsions: Formulation, Fabrication, Properties, Performance, Biological Fate, and Potential Toxicity. *Crit. Rev. Food Sci. Nutr.* **2011**, *51*, 285−330.
(26) Rodriguez-Lopez, G.; O'Neil Williams, Y.; Toro-Mendoza, J. Individual and Collective Behavior of Emulsion Droplets Undergoing Ostwald Ripening. *Langmuir* **2019**, *35*, 5316−5323.
(27) Thompson, K. L.; Derry, M. J.; Hatton, F. L.; Armes, S. P. Long-Term Stability of n-Alkane-in-Water Pickering Nanoemulsions: Effect of Aqueous Solubility of Droplet Phase on Ostwald Ripening. *Langmuir* **2018**, *34*, 9289−9297.
(28) Nazarzadeh, E.; Anthonypillai, T.; Sajjadi, S. On the growth mechanisms of nanoemulsions. *J. Colloid Interface Sci.* **2013**, *397*, 154−162.
(29) Wooster, T. J.; Golding, M.; Sanguansri, P. Impact of Oil Type on Nanoemulsion Formation and Ostwald Ripening Stability. *Langmuir* **2008**, *24*, 12758−12765.
(30) Mun, S.; McClements, D. J. Influence of Interfacial Characteristics on Ostwald Ripening in Hydrocarbon Oil-in-Water Emulsions. *Langmuir* **2006**, *22*, 1551−1554.
(31) Egger, H.; McGrath, K. M. Aging of oil-in-water emulsions: The role of the oil. *J. Colloid Interface Sci.* **2006**, *299*, 890−899.
(32) Solans, C.; Izquierdo, P.; Nolla, J.; Azemar, N.; Garcia-Celma, M. J. Nano-emulsions. *Curr. Opin. Colloid Interface Sci.* **2005**, *10*, 102−110.
(33) Jiao, J.; Burgess, D. J. Ostwald ripening of water-in-hydrocarbon emulsions. *J. Colloid Interface Sci.* **2003**, *264*, 509−516.
(34) Kabalnov, A. Ostwald Ripening and Related Phenomena. *J. Dispersion Sci. Technol.* **2001**, *22*, 1−12.
(35) Weiss, J.; Canceliere, C.; McClements, D. J. Mass Transport Phenomena in Oil-in-Water Emulsions Containing Surfactant Micelles: Ostwald Ripening. *Langmuir* **2000**, *16*, 6833−6838.
(36) De Smet, Y.; Deriemaeker, L.; Finsy, R. Ostwald Ripening of Alkane Emulsions in the Presence of Surfactant Micelles. *Langmuir* **1999**, *15*, 6745−6754.
(37) Taylor, P. Ostwald ripening in emulsions. *Adv. Colloid Interface Sci.* **1998**, *75*, 107−163.
(38) Taylor, P.; Ottewill, R. H. The formation and ageing rates of oil-in-water miniemulsions. *Colloids Surf., A* **1994**, *88*, 303−316.
(39) McClements, D. J.; Dungan, S. R.; German, J. B.; Kinsella, J. E. Evidence of Oil Exchange between Oil-in-Water Emulsion Droplets Stabilized by Milk Proteins. *J. Colloid Interface Sci.* **1993**, *156*, 425−429.
(40) Kabal'nov, A. S.; Pertzov, A. V.; Shchukin, E. D. Ostwald ripening in two-component disperse phase systems: Application to emulsion stability. *Colloids Surf.* **1987**, *24*, 19−32.
(41) Davis, S. S.; Round, H. P.; Purewal, T. S. Ostwald ripening and the stability of emulsion systems: an explanation for the effect of an added third component. *J. Colloid Interface Sci.* **1981**, *80*, 508−511.
(42) Buscall, R.; Davis, S. S.; Potts, D. C. The effect of long-chain alkanes on the stability of oil-in-water emulsions. The significance of ostwald ripening. *Colloid Polym. Sci.* **1979**, *257*, 636−644.
(43) Hunter, S. J.; Penfold, N. J. W.; Chan, D. H.; Mykhaylyk, O. O.; Armes, S. P. How Do Charged End-Groups on the Steric Stabilizer Block Influence the Formation and Long-Term Stability of Pickering Nanoemulsions Prepared Using Sterically Stabilized Diblock Copolymer Nanoparticles? *Langmuir* **2020**, *36*, 769−780.
(44) Dieng, S. M.; Anton, N.; Bouriat, P.; Thioune, O.; Sy, P. M.; Massaddeq, N.; Enharrar, S.; Diarra, M.; Vandamme, T. Pickering nano-emulsions stabilized by solid lipid nanoparticles as a temperature sensitive drug delivery system. *Soft Matter* **2019**, *15*, 8164−8174.
(45) Lee, Y.-T.; Li, D. S.; Ilavsky, J.; Kuzmenko, I.; Jeng, G.-S.; O'Donnell, M.; Pozzo, L. D. Ultrasound-based formation of nano-Pickering emulsions investigated via in-situ SAXS. *J. Colloid Interface Sci.* **2019**, *536*, 281−290.
(46) Hunter, S. J.; Abu Elella, M. H.; Johnson, E. C.; Taramova, L.; Brotherton, E. E.; Armes, S. P.; Khutoryanskiy, V. V.; Smallridge, M. J. Mucoadhesive pickering nanoemulsions via dynamic covalent chemistry. *J. Colloid Interface Sci.* **2023**, *651*, 334−345.
(47) Charleux, B.; Delaittre, G.; Rieger, J.; D'Agosto, F. Polymerization-Induced Self-Assembly: From Soluble Macromolecules to Block Copolymer Nano-Objects in One Step. *Macromolecules* **2012**, *45*, 6753−6765.
(48) Warren, N. J.; Armes, S. P. Polymerization-Induced Self-Assembly of Block Copolymer Nano-objects via RAFT Aqueous Dispersion Polymerization. *J. Am. Chem. Soc.* **2014**, *136*, 10174−10185.
(49) Derry, M. J.; Fielding, L. A.; Armes, S. P. Polymerization-induced self-assembly of block copolymer nanoparticles via RAFT non-aqueous dispersion polymerization. *Prog. Polym. Sci.* **2016**, *52*, 1−18.
(50) Lowe, A. B. RAFT alcoholic dispersion polymerization with polymerization-induced self-assembly. *Polymer* **2016**, *106*, 161−181.
(51) Canning, S. L.; Smith, G. N.; Armes, S. P. A Critical Appraisal of RAFT-Mediated Polymerization-Induced Self-Assembly. *Macromolecules* **2016**, *49*, 1985−2001.

https://doi.org/10.1021/acs.langmuir.3c03423
Langmuir 2024, 40, 3702−3714

(52) Penfold, N. J. W.; Yeow, J.; Boyer, C.; Armes, S. P. Emerging Trends in Polymerization-Induced Self-Assembly. *ACS Macro Lett.* **2019**, *8*, 1029−1054.
(53) D'Agosto, F.; Rieger, J.; Lansalot, M. RAFT-Mediated Polymerization-Induced Self-Assembly. *Angew. Chem., Int. Ed.* **2020**, *59*, 8368−8392.
(54) Hunter, S. J.; Armes, S. P. Pickering Emulsifiers Based on Block Copolymer Nanoparticles Prepared by Polymerization-Induced Self-Assembly. *Langmuir* **2020**, *36*, 15463−15484.
(55) Zhou, W.; Qu, Q.; Xu, Y.; An, Z. Aqueous Polymerization-Induced Self-Assembly for the Synthesis of Ketone-Functionalized Nano-Objects with Low Polydispersity. *ACS Macro Lett.* **2015**, *4*, 495−499.
(56) Blanazs, A.; Ryan, A. J.; Armes, S. P. Predictive Phase Diagrams for RAFT Aqueous Dispersion Polymerization: Effect of Block Copolymer Composition, Molecular Weight, and Copolymer Concentration. *Macromolecules* **2012**, *45*, 5099−5107.
(57) Sugihara, S.; Armes, S. P.; Blanazs, A.; Lewis, A. L. Non-spherical morphologies from cross-linked biomimetic diblock copolymers using RAFT aqueous dispersion polymerization. *Soft Matter* **2011**, *7*, 10787−10793.
(58) Li, Y.; Armes, S. P. RAFT Synthesis of Sterically Stabilized Methacrylic Nanolatexes and Vesicles by Aqueous Dispersion Polymerization. *Angew. Chem., Int. Ed.* **2010**, *49*, 4042−4046.
(59) Brotherton, E. E.; Hatton, F. L.; Cockram, A. A.; Derry, M. J.; Czajka, A.; Cornel, E. J.; Topham, P. D.; Mykhaylyk, O. O.; Armes, S. P. In Situ Small-Angle X-ray Scattering Studies During Reversible Addition−Fragmentation Chain Transfer Aqueous Emulsion Polymerization. *J. Am. Chem. Soc.* **2019**, *141*, 13664−13675.
(60) Hatton, F. L.; Lovett, J. R.; Armes, S. P. Synthesis of well-defined epoxy-functional spherical nanoparticles by RAFT aqueous emulsion polymerization. *Polym. Chem.* **2017**, *8*, 4856−4868.
(61) Mable, C. J.; Warren, N. J.; Thompson, K. L.; Mykhaylyk, O. O.; Armes, S. P. Framboidal ABC triblock copolymer vesicles: a new class of efficient Pickering emulsifier. *Chem. Sci.* **2015**, *6*, 6179−6188.
(62) Chan, D. H. H.; Hunter, S. J.; Neal, T. J.; Lindsay, C.; Taylor, P.; Armes, S. P. Adsorption of sterically-stabilized diblock copolymer nanoparticles at the oil−water interface: effect of charged end-groups on interfacial rheology. *Soft Matter* **2022**, *18*, 6757−6770.
(63) Cunningham, V. J.; Alswieleh, A. M.; Thompson, K. L.; Williams, M.; Leggett, G. J.; Armes, S. P.; Musa, O. M. Poly(glycerol monomethacrylate)−Poly(benzyl methacrylate) Diblock Copolymer Nanoparticles via RAFT Emulsion Polymerization: Synthesis, Characterization, and Interfacial Activity. *Macromolecules* **2014**, *47*, 5613−5623.
(64) Akpinar, B.; Fielding, L. A.; Cunningham, V. J.; Ning, Y.; Mykhaylyk, O. O.; Fowler, P. W.; Armes, S. P. Determining the Effective Density and Stabilizer Layer Thickness of Sterically Stabilized Nanoparticles. *Macromolecules* **2016**, *49*, 5160−5171.
(65) Chan, D. H. H.; Cockram, A. A.; Gibson, R. R.; Kynaston, E. L.; Lindsay, C.; Taylor, P.; Armes, S. P. RAFT aqueous emulsion polymerization of methyl methacrylate: observation of unexpected constraints when employing a non-ionic steric stabilizer block. *Polym. Chem.* **2021**, *12*, 5760−5769.
(66) Ilavsky, J.; Jemian, P. R. Irena: tool suite for modeling and analysis of small-angle scattering. *J. Appl. Crystallogr.* **2009**, *42*, 347−353.
(67) Pedersen, J. S. Form factors of block copolymer micelles with spherical, ellipsoidal and cylindrical cores. *J. Appl. Crystallogr.* **2000**, *33*, 637−640.
(68) Pedersen, J. S.; Gerstenberg, M. C. Scattering Form Factor of Block Copolymer Micelles. *Macromolecules* **1996**, *29*, 1363−1365.
(69) Balmer, J. A.; Armes, S. P.; Fowler, P. W.; Tarnai, T.; Gáspár, Z.; Murray, K. A.; Williams, N. S. J. Packing Efficiency of Small Silica Particles on Large Latex Particles: A Facile Route to Colloidal Nanocomposites. *Langmuir* **2009**, *25*, 5339−5347.
(70) Lifshitz, I. M.; Slyozov, V. V. The kinetics of precipitation from supersaturated solid solutions. *J. Phys. Chem. Solids* **1961**, *19*, 35−50.
(71) Wagner, C. Theorie der Alterung von Niederschlägen durch Umlösen (Ostwald-Reifung). *Z. Elektrochem. Ber. Bunsenges. Phys. Chem.* **1961**, *65*, 581−591.
(72) Higuchi, W. I.; Misra, J. Physical Degradation of Emulsions Via the Molecular Diffusion Route and the Possible Prevention Thereof. *J. Pharm. Sci.* **1962**, *51*, 459−466.
(73) Delmas, T.; Piraux, H.; Couffin, A.-C.; Texier, I.; Vinet, F.; Poulin, P.; Cates, M. E.; Bibette, J. How To Prepare and Stabilize Very Small Nanoemulsions. *Langmuir* **2011**, *27*, 1683−1692.
(74) Koroleva, M. Y.; Yurtov, E. V. Effect of ionic strength of dispersed phase on Ostwald ripening in water-in-oil emulsions. *Colloid J.* **2003**, *65*, 40−43.
(75) Thomson, W. LX. On the equilibrium of vapour at a curved surface of liquid. *Lond., Edinburgh, Dublin Philos. Mag. J. Sci.* **1871**, *42*, 448−452.
(76) Gupta, A.; Eral, H. B.; Hatton, T. A.; Doyle, P. S. Nanoemulsions: formation, properties and applications. *Soft Matter* **2016**, *12*, 2826−2841.
(77) Li, P.-H.; Chiang, B.-H. Process optimization and stability of d-limonene-in-water nanoemulsions prepared by ultrasonic emulsification using response surface methodology. *Ultrason. Sonochem.* **2012**, *19*, 192−197.
(78) Teng, F.; He, M.; Xu, J.; Chen, F.; Wu, C.; Wang, Z.; Li, Y. Effect of ultrasonication on the stability and storage of a soy protein isolate-phosphatidylcholine nanoemulsions. *Sci. Rep.* **2020**, *10*, No. 14010.
(79) Taylor, P. Ostwald ripening in emulsions: estimation of solution thermodynamics of the disperse phase. *Adv. Colloid Interface Sci.* **2003**, *106*, 261−285.
(80) Kabalnov, A. S.; Makarov, K. N.; Pertzov, A. V.; Shchukin, E. D. Ostwald ripening in emulsions: 2. Ostwald ripening in hydrocarbon emulsions: Experimental verification of equation for absolute rates. *J. Colloid Interface Sci.* **1990**, *138*, 98−104.
(81) Schatzberg, P. Solubilities Of Water In Several Normal Alkanes From C7 tO C161. *J. Phys. Chem. A* **1963**, *67*, 776−779.
(82) Hildebrand, J. H.; Scott, R. L. *Solubility of Non-Electrolytes*; Reinhold Publishing Corporation: New York, 1950.
(83) Stevenson, R. L.; LaBracio, D. S.; Beaton, T. A.; Thies, M. C. Fluid Phase Equilibria and critical phenomena for the dodecane-water and squalane-water systems at elevated temperatures and pressures. *Fluid Phase Equilib.* **1994**, *93*, 317−336.

NOTE ADDED AFTER ASAP PUBLICATION

This paper was published ASAP on February, 5, 2024, with an error in the Results and Discussion section. The corrected version was reposted on February 6, 2024.

https://doi.org/10.1021/acs.langmuir.3c03423
Langmuir 2024, 40, 3702−3714